Experimental analysis of heat transfer and friction for three sides roughened solar air heater

Vikash Kumar[1,*], Laljee Prasad[2]

1. Dept. of Mechanical Engineering, Malla Reddy College of Engineering, Secunderabad-500100, India

2. Dept. of Mechanical Engineering, NIT Jamshedpur, Jharkhand-831014, India

vikashism2012@gmail.com

ABSTRACT. *This paper deals with the results so obtained after conducting exhaustive experimentation on 1 & 3-sides concave dimple roughened SAH in terms of Nusselt number (Nu) & friction factor (f). The geometrical & flow parameters were used as dimensionless ratio as relative dimple pitch (p/e), relative dimple height (e/Dh), relative dimple depth (e/d) and 'Re' in the range of 8-15, 0.018-0.045, 1-2 and 2500-13500 respectively. For various sets of roughness parameters, there exists an optimum roughness parameter, either side of which heat transfer rate decreased. The optimum roughness parameters found under present investigation is p/e=12, e/Dh=0.036 and e/d=1.5. The maximum rise in 'Nu' for varying 'p/e', 'e/Dh' & 'e/d' was respectively found to be of the order of 2.6 to 3.55 times, 1.91 to 3.42 times and 3.09 to 3.94 times than one side concave dimple roughened duct for the parameters range investigated. The maximum rise in friction factor of 3-sides concave dimple over those of 1-side roughened ones for varying 'p/e', 'e/Dh' & 'e/d' was respectively found to be as 1.62 to 2.79 times, 1.52 to 2.34 times and 2.21 to 2.56 times.*

RÉSUMÉ. *Cet article traite des résultats ainsi obtenus après avoir mené une expérimentation exhaustive sur des SAH dépolies concaves à 1 et 3 côtés, en termes de nombre de Nusselt (Nu) et de facteur de friction (f). Les paramètres géométriques et de débit ont été utilisés comme rapport sans dimension: pas de fossé relatif; (p / e), hauteur de la fossette relative (e / Dh), Profondeur de fossette relative (e / d) et «Re» dans la plage de 8-15, 0,018-0,045, 1-2 et 2500-13500 respectivement. Pour divers ensembles de paramètres de rugosité, il existe un paramètre de rugosité optimal, dans lequel le taux de transfert de chaleur a diminué. Les paramètres de rugosité optimaux trouvés dans les recherches actuelles sont p/e=12, e/Dh=0.036 et e/d=1.5. L'augmentation maximale dans le 'Nu' pour les variables 'p / e', 'e / Dh' et 'e / d' s'est avérée être respectivement de l'ordre de 2,6 à 3,55 fois, de 1,91 à 3,42 fois et de 3,09 à 3,94 fois supérieure à celle du canal rugueux concave d'un côté pour la plage de paramètres étudiée. L'augmentation maximale du facteur de frottement de la fossette concave à 3 côtés par rapport à ceux des côtés rugueux à 1* *côté pour une variation de 'p/e', 'e/D_h' & 'e/d' était respectivement de 1,62 à 2,79 1,52 à 2,34 fois et 2,21 à 2,56 fois.*

KEYWORDS: *concave dimple, relative dimple pitch, relative dimple height, relative dimple depth, nusselt number,; friction factor.*

MOTS-CLÉS: *fossette concave, pas de fosse relatif, hauteur de la fossette relative, profondeur de fossette relative, numero de nusselt, facteur de frictions.*

DOI:10.3166/ACSM.41.75-107 © 2017 Lavoisier

1. Introduction

Renewable energy sources have a huge impact on the power need of human beings. Based on REN21's 2016 report, renewable energy sources contribution to human's global energy consumption was 19.2% and 23.7% towards power generation in 2014 and 2015 respectively. The consumption shares 8.9% from biomass sources, 4.2% as thermal sources viz. modern bio-mass, geo-thermal and solar thermal energy), 3.9% hydel power and 2.2% is the power generation using wind, solar energy, geo-thermal, and bio-mass sources. As per data available worldwide, till 2015, a little over 50% power generating plants have switched to renewable resources (Armaroli and Balzani, 2016). [1]

1.1. Solar energy applications

Generally solar energy can be used in two ways: electricity and heat. Solar heating technology uses the thermal energy in sun waves to heat water or air for applications such as space heating, water heating, and cooling for homes and businesses. Solar thermal energy can also be harvested for power generation such as concentrating solar power plant. Solar photovoltaic technology converts solar energy into electricity using semiconducting material solar cell (Sukhatme, 1986; Duffie and Beckman, 1991).

Using artificial roughness of various shape geometry and orientation has been proven to be the most effective method to harness solar energy (Prasad and Saini, 1988). The heat transfer and friction characteristics of non-roughened SAH are poor because of low vale of heat transfer convection co-efficient of air and also because air can't be used as a medium to store heat because of its low thermal heat capacity. The presence of laminar sub-layer in the turbulent zone of heat transferring surface also prevent heat to be transferred from heated collector to the relatively cooler underside flowing air (Edwards and Sheriff, 1961). Literature upon SAH clearly suggest that many efforts were made towards increasing the heat transfer rate from absorber to air by artificially destroying laminar sub-layer creating roughness/disturbances on the collector's surface. These roughness/disturbances

1. Source: http://www.renewindians.com/2013/02/indian-renewable-installed-capacity-has-reached-27.7GW.html

provided on collector's surface destroy the laminar sub-layer, give rise to local wall turbulence because of flow separation and reattachment amongst consecutive roughness elements that leads in reducing thermal resistance & largely contributes to heat transfer augmentation.

However, using roughness/disturbances in the air flow path will generate higher losses due to friction leading excessive power requirement from the blower to ensure the desired flow rate inside roughened duct (Akhtar and Mullick, 2012; Pillar and Agarwal, 1981; Varun *et al*., 2007; Ahn, 2001; Karwa *et al*., 2001; Dippreyy and Sabersky, 1963; Firth and Meyer, 1983; Nguyen *et al*., 1989; Han *et al*., 1991). A large number of researchers have worked in this area concluded that these roughness should be provided very close to the heat transfer surface (height/depth of roughness element shouldn't exceed laminar sublayer thickness) because if the roughness's dimension exceed laminar sub-layer thickness, there will be a drastic increase in pumping power requirement, reducing the overall performance of the roughened SAH duct (Singh *et al.*, 2012; Yadav and Bhagoria, 2014; Singh *et al*., 2015).

1.2. Literature on artificially roughened SAHs

Prasad and Saini (1988) concluded that there is an optimum arrangement of 'p/e' and 'e/D_h' that will give maximum possible enhancement in heat transfer based upon their investigations conducted upon transverse rib roughened SAH. Prasad and Mullick (1985) recommended using artificial roughness as small diameter wires attached to SAH to improve its thermal performance. Gupta *et al*. (1997) worked on the 'Nu & f' characteristics of artificial roughness in form of inclined wires. They reported that 60° angle of attack produced maximum heat transfer where as 70° showed highest friction factor. Han *et al*. (1985) studied the effect of relative rib pitch and height on 'Nu & f' for 'Re' of 7,000-90,000, 'p/e' of 10-40 & 'e/D_h' of 0.021-0.063. During investigation it was observed that maximum friction & Stanton Number occurred at 'p/e' value of 10. Naphon (2008) experimentally studied 'Nu and f' characteristics of two opposite corrugated plates with tilt angles of 20˚, 40˚ & 60˚ and found that due to the breaking and destabilizing in the thermal boundary zone, the corrugated plate has high impact 'Nu and f' enhancement. Chang *et al*. (2008) studied the effect of V-shaped ribs and deepened scales and found that enhancement in heat transfer ratios were 9.5-13.6 and 9-12.3 with forward and backward flows respectively for viscous flow and 6.8-6.3 & 5.7-4.3 for turbulent flow. Bhagoria *et al*. (2002) concluded that 'Nu and f' characteristics in a transverse wedge roughened SAH increased by an amount of 2.4 & 5.3 times the non-roughened duct under the investigated parameter of 'Re', 'e/D_h' & wedge angle varying from 3000-18000, 0.015-0.033 and 8-12 respectively. Patil *et al*. (2012) investigated multi v-shaped rib with gaps as roughness element & analyzed its effects on 'Nu and f' characteristics. The 'Nu & f' increased by an amount 6.32-6.12 times compared to non-roughened duct. Skullong and Promvonge (2014) conducted investigations upon deltawinglet type vortex generators (DWs) roughness element and analyzed their effect upon 'Nu and f' characteristics. The investigation revealed that 60° DW-E at Rp=1 yielded maximum 'Nu and f whereas the 30° DW-E at Rp=1 showed higher thermal performance than the others. Leontiev *et al*. experimentally studied about heat transfer and the drag on surfaces coated with dimples of six different shapes namely, spherical, oval, teardrop dimples, spherical dimples with rounded edges, turned teardrop dimples, and dimples obtained by milling a sphere along a circular arc. The 'Re' ranged $0.2x10^6$-7x106. The models for which the dead-air zone is minimum, or almost absent, (teardrop dimples) ensure the greatest increase in the heat transfer.

It appears from literature that most of the roughness provided on absorber was limited to one side while three remaining sides were insulated. If roughness provided is on all three sides, (2 side walls and 1 top wall), they can participate in the heat transfer augmentation process accompanied by the slightest increase in pressure drop resulting in an appreciable enhancement in heat transfer. The present investigation accommodates the provision of roughness in the form of concave dimple geometry to avoid manufacturing complexities on three sides of the absorber while one side being insulated and to analyze the effects of relative dimple pitch ('p/e'), relative dimple height ('e/D_h') & relative dimple depth (e/d) on heat transfer and friction characteristics.

2. Equipments and methods

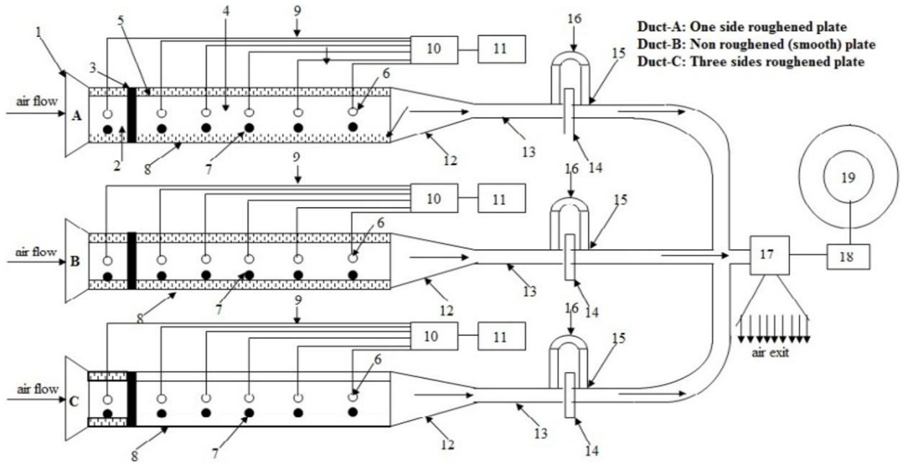

Note: 1. Trapezoidal air inlet; 2. Non-roughened section; 3. Insulation; 4. Roughened duct section; 5. Insulation; 6. Thermocouple; 7. Thermometer; 8. Glass covers; 9. Copper wire; 9. Selector switch; 10. Digital voltmeter; 11. Converging section; 12. Cylindrical pipe; 13. Orifice-plate; 14. Flange couplings; 15. U-tube manometer; 16. Blower; 17. Motor; 18. Auto-Variac

Figure 1. Schematics of test set-up

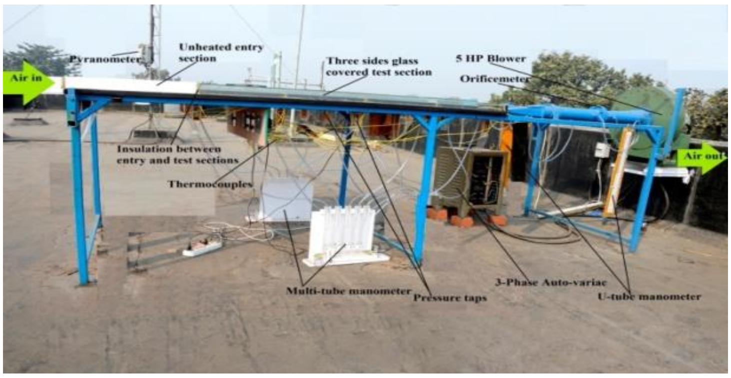

Figure 2. Photograph of test setup

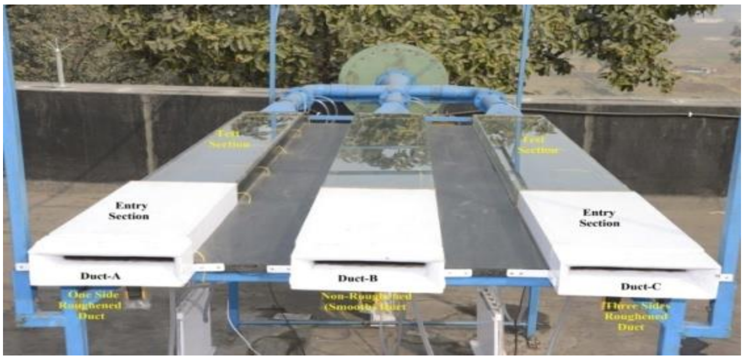

Figure 3. Front view of test set-up

Figure 4. Photograph of one and three sides roughened absorber plates

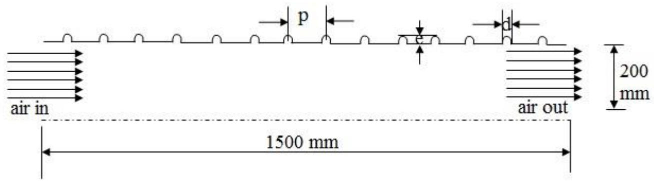

Figure 5. Sectional view of a concave dimple roughened absorber plate

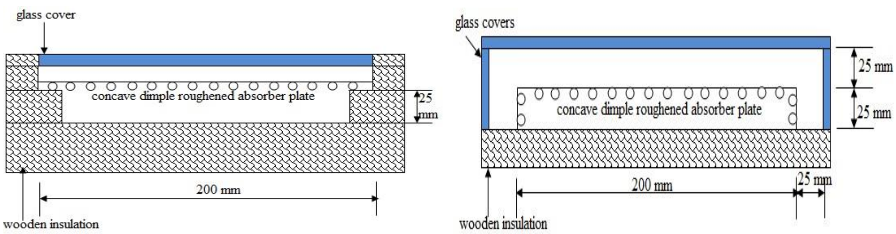

Figure 6. Schematics of one and three sides artificially roughened ducts

Figure 1 shows the schematic diagram of the test set-up used under present investigation. Figure 2 & 3 shows the actual photograph of the experimental set-up. Figure 4 shows the actual photograph of 1 & 3-sides concave dimple roughened plates. Figure 5 shows the sectional view of concave dimple roughness geometry. Under present investigation, roughness parameters such as dimple pitch (p), dimple height/depth (e) and dimple diameter (d) have been used as dimensionless ratio as relative dimple pitch (p/e), relative dimple height (e/D_h) and relative dimple depth (e/d). One side and three sides roughened plates with concave dimple geometry crafted on its flow-facing side have been fabricated as per ASHRAE standard (ASHRAE Standard 93-97, 1977). An experimental set-up placed in actual outdoor condition was used to test these roughened plates.

The present experimental investigations make use of only two ducts with the facility to accommodate 1 & 3-sides roughened absorbers. The two ducts have been made similar in all dimensions to achieve direct comparison between the 'Nu & f' characteristics. The two ducts had provision to suck ambient air separately but exhausted it into a single outlet. A (2.13 x 0.63) m wooden piece 25 mm thick acted as the common bottom plate of the ducts, the side walls of 50 mm x 50 mm wooden piece for one side artificially roughened duct with top side glass cover. For 3-sides artificially roughened duct, three sides glass covers (250 mm x 50 mm x 50 mm) and bottom side was of wooden insulation. 25 mm air gap provided between bottom & absorber plate for each duct resulted in the duct cross section of 200 mm x 25 mm each. Figure 6 shows the schematic view of the two ducts used under present investigation.

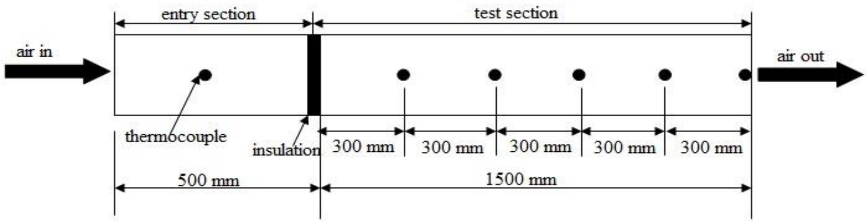

Figure 7. Thermocouple positioning on one side roughened absorber plate

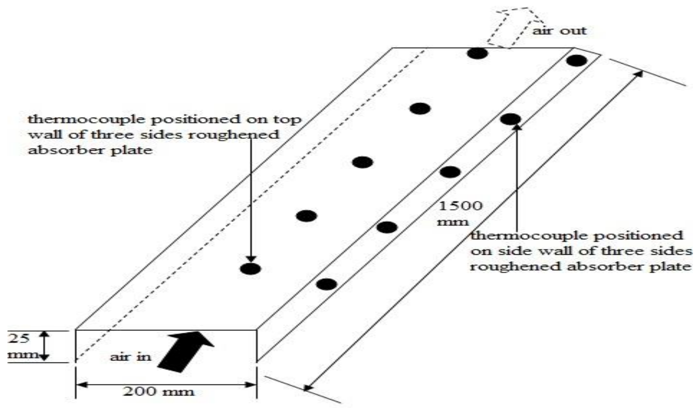

Figure 8. Thermocouple positioning on three sides roughened absorber plate

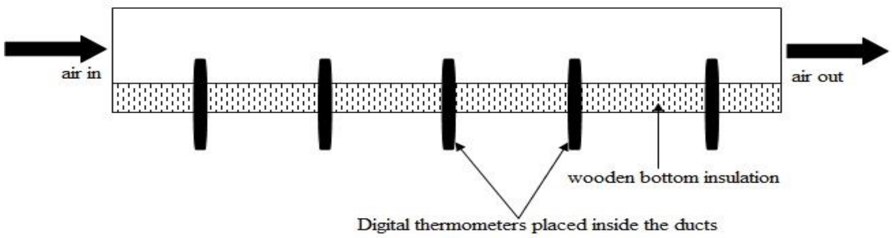

Figure 9. Digital thermometers placed inside air flow duct test section

From the total duct length of 2130 mm each, only the test section of 1500 mm was instrumented and 630 mm length on the entry side serves as entry length for stabilization of flow. The calibrated copper-constantan thermocouples (28 SWG) with digitalmicro-voltmeter, output in ˚C having accuracy of 0.1 °C, were used to measure collector's temperatures at various locations. Eighteen thermocouples have been soldered on top surface of the collector to record collector's temperatures. The positioning of thermocouples is depicted in Figure 7 & 8. Digital thermometer's position has been shown in Figure 9.

The flow and roughness geometry parameters used under present study is presented in Table 1.

Table 1. Range of flow and geometrical parameters

Flow and Geometrical Parameters (Variable Value Range)				
1.	Relative roughness pitch	p/e	-	8-15
2.	Relative roughness height	e/D_h	-	0.018-0.045
3.	Depth to Diameter ratio	e/d	-	1-2
4.	Reynolds number	Re	-	2500-13500
5.	Intensity of solar radiation	I	W/m^2	720-980
6.	Atmospheric temperature	T_a	˚C	24-44
7.	Wind velocity	W_v	m/s	0.2-3.5

3. Data reduction

Heated air & collector's temperatures were recorded at different locations in the duct as described earlier were used, for determining the values of different parameters. The following equations were used for calculating the plate meantemperature (T_{pm}), air meantemperature (T_{fm}), flow rate ($\dot{m}$), heat transferred to the under flowing air (Q_u) & heat transfer convection coefficient (h).

3.1. Mean air and plate temperatures

The mean temperatures, T_{pm} & T_{fm} are simply the arithmetic mean of the noted values of temperatures at different locations in between the inlet & exit of the test section. Thus:

$$\left(T_{pm}\right)_{3r} = \frac{T_1 + T_2 + \dots\dots\dots\dots\dots\dots + T_{12}}{12} \tag{1}$$

$$\left(T_{pm}\right)_{1r} = \frac{T_1 + T_2 + \dots\dots\dots + T_6}{6} \tag{2}$$

$$\left(T_{fm}\right)_{3r} = \frac{T_1 + T_6}{2} \tag{3}$$

$$\left(T_{fm}\right)_{1r} = \frac{T_1 + T_6}{2} \tag{4}$$

3.2. Mass flow rate measurement

Using the pressure drop measurement across the orifice, the flow rate of air under roughened plate is calculated as:

$$\dot{m} = C_d A_o \left[\frac{2\rho \Delta p_o}{1-\beta^4} \right]^{0.5} \tag{5}$$

3.3. Friction factor

The ‘f’ value is calculated using pressure drop $(\Delta p)_d$, across test section length, L of 1500 mm (between the two points at 500 mm and 1500mm across the test length with pressure taps inserted at five different locations, each at a gap of 300 mm as shown in Figure. 3.15) and the mass flow rate, $\dot{m}$ as:

$$f = \frac{(\Delta p)_d \, D_h}{2\rho L {v_d}^2} \tag{6}$$

where, D_h: hydraulic diameter for the duct and is evaluated as:

$$D_h = \frac{4WH}{[2(W+H)]} \tag{7}$$

and, v_d is the flow velocity of air flowing inside the roughened duct.

3.4. Reynolds number

The ‘Re’ is calculated using:

$$\mathrm{Re} = \frac{v_d D_h}{\upsilon} \tag{8}$$

3.5. Heat transfer coefficient

Useful heat gain of air is given by:

$$Q_u = \dot{m} C_p (T_6 - T_1) \tag{9}$$

The heat transfer coefficient for the heated test section has been calculated from:

$$h = \frac{Q_u}{A_p (T_{pm} - T_{fm})} \tag{10}$$

where, A_p is the heat transfer area, assumed corresponding one side roughened plate area.

3.6. Nusselt number

The heat transfer coefficient is used to determine the 'Nu' and is determined as:

$$Nu = \frac{hD_h}{k} \tag{11}$$

where, 'k': thermal conductivity of the air

4. Validation of experimental data

Apart from three sides concave dimple roughened duct, the experiments were also carried out for one side concave dimple roughened duct similar to those of Saini and Verma (2008) to compare the values of 'Nu' & 'f' obtained from the experiment with the values obtained from the correlations of 'Nu' & 'f' suggested by Saini and Verma. The 'Nu' & 'f' for a one side dimple roughened rectangular duct is given as:

$$\left(Nu\right)_{1r} = 5.2\times10^{-4}\times(\mathrm{Re})^{1.27}\times\left(\frac{p}{e}\right)^{1.15}\times\left(\frac{e}{D_h}\right)^{0.0333}\left[\exp\times(-2.12)\left(\log\times\left(\frac{p}{e}\right)\right)^{2}\right]$$
$$\left[\exp\times(-1.30)\left(\log\times\left(\frac{e}{D_h}\right)\right)^{2}\right] \tag{12}$$

$$f_{1r} = 0.642\times\mathrm{Re}^{-0.423}\times\left(\frac{p}{e}\right)^{-0.465}\times\left(\frac{e}{D_h}\right)^{-0.0214}\left[\exp\times\left(0.054\right)\left(\log\times\left(\frac{p}{e}\right)\right)^{2}\right]$$
$$\left[\exp\times\left(0.840\right)\left(\log\times\left(\frac{e}{D_h}\right)\right)^{2}\right] \tag{13}$$

Since one side dimple roughened SAH data compared well with a similar model taken by Saini & Verma, therefore, the results for three sides roughened ones are worth to be valid and hence been utilized further. Figure 10 shows the comparison of experimental values 'Nu' & 'f' with 'Nu' & 'f' obtained from the correlations as suggested by Saini and Verma. The mean deviation in experimental & estimated values of 'Nu' & 'f' was found as ±3.7% for 'Nu' & ± 4.5% for 'f'.

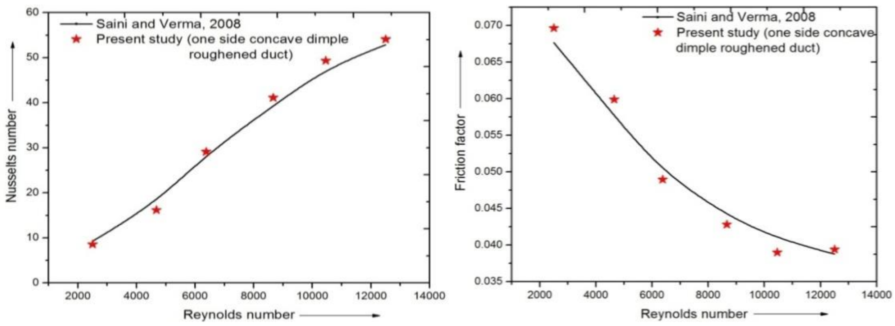

Figure 10. Comparison b/w experimental and calculated values of 'Nu' & 'f' for one side concave dimple roughened SAH

4.1. Uncertainty analysis

Table 2. Uncertainties in measurement of various parameters

S. No.	Name of parameter	Uncertainty range (%)
1.	Area of absorber plate (A_p)	0.07
2.	Cross sectional area of duct (A)	0.16
3.	Area of orifice meter (A_o)	0.21
4.	Hydraulic diameter	0.23
5.	Density	0.106
6.	Mass flow rate	0.84
7.	Velocity of air through test section	0.86
8.	Reynolds Number (Re)	0.9
9.	Heat transfer co-efficient	3.724
10.	Nusselt number (Nu)	4.167
11.	Friction factor (f)	4.389
12.	Useful heat gain	3.14
13.	Thermal Efficiency	3.14

Based on the method of Kline and McClinLock (1953) of the uncertainties associated with various parameters, the uncertainties have been discussed and the elaborated form is given in Appendix-A. Uncertainties values of various parameters are given in Table 2.

5. Results and discussions

The roughness geometry's shape and orientation have a major impact on the 'Nu' & 'f' characteristics by altering turbulence. Under present experimental studies, effect of concave dimple geometry's parameters such as 'p/e', 'e/D_h' & 'e/d' on 'Nu' has been studied exhaustively and presented as rise in 'Nu' with mass flow rate of air (Reynolds number). The roughness parameters should be selected in such a way that maximum heat transfer can be obtained at the cost of minimum rise in pressure drop.

5.1. Effect of ‘p/e’ on ‘Nu’

Figure 11 shows the variation of ‘Nu’ as a function of ‘p/e’ & ‘Re’ for fixed ‘e/D_h’=0.018 & ‘e/d’=1. The maximum & minimum value for ‘Nu’ is obtained at ‘p/e’ of 12 & 8 respectively for the entire values of ‘Re’ investigated. Similarly, Figures 12 to 14 have been drawn at varying ‘p/e’ for different sets of values of ‘e/D_h’ and dimple depth to diameter (relative dimple depth) ratio. It was observed that for all the values of ‘Re’, ‘Nu’ increased with increasing in ‘p/e’ value but only upto ‘p/e’ of 12 beyond which ‘Nu’ started decreasing with respect to mass flow rate. Thus, it is discovered that the maximum value for ‘Nu’ is obtained for ‘p/e’ value between 10-12. The enhancement in ‘Nu’ based on Nusselt number enhancement ratio (Nu_{3r}/Nu_{1r}) lies in the range of 2.26 times to 3.55 times to that of the one side concave dimple roughened duct under similar operating conditions.

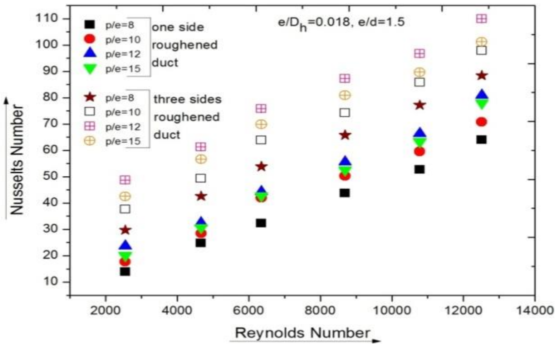

Figure 11. Variation in ‘Nu’ with ‘Re’ for different ‘p/e’ & for fixed ‘e/D_h’=0.018 & ‘e/d’=1.5

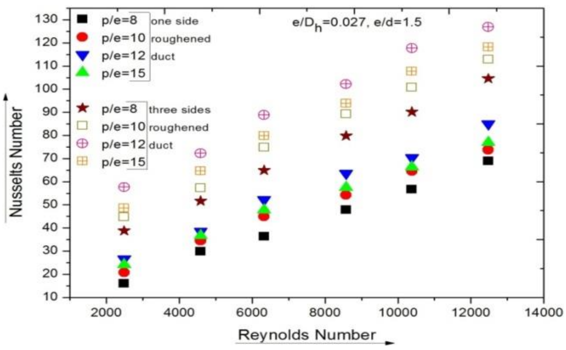

Figure 12. Variation in ‘Nu’ with ‘Re’ for different ‘p/e’ & for fixed ‘e/D_h’=0.027 & ‘e/d’=1.5

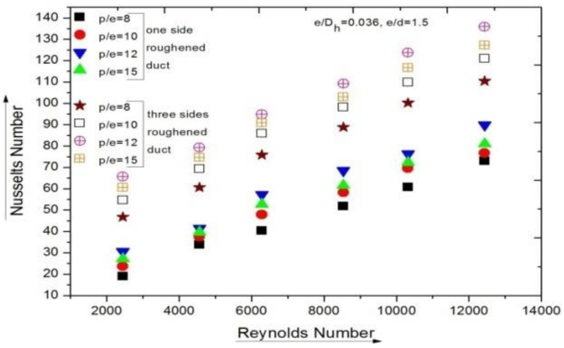

Figure 13. Variation in ‘Nu’ with ‘Re’ for different ‘p/e’ & for fixed ‘e/D_h’=0.036 & ‘e/d’=1.5

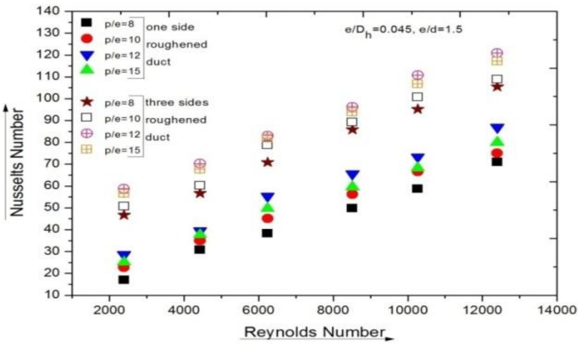

Figure 14. Variation in ‘Nu’ with ‘Re’ for different ‘p/e’ & for fixed ‘e/D_h’=0.045 & ‘e/d’=1.5

5.2. Effect of ‘e/D_h’ on ‘Nu’

Different ‘e/D_h’ of 0.018, 0.027, 0.036 and 0.045 & constant ‘p/e’ of 12 & ‘e/d’ of 1.5 has been considered. Similarly, Figures 15 to 18 have been drawn at varying e/D_h for different sets of values of relative roughness pitch and dimple depth to diameter ratio. For all ‘Re’ values, ‘Nu’ is higher for three sides concave dimple roughened duct compared to that of one side concave dimple roughened duct. ‘Nu’ increases as ‘e/D_h’ increases but only upto the value of 0.036 beyond which it tends to decreases with further increase in the value of ‘e/D_h’. The ‘Nu’ enhancement based on 'Nu' enhancement ratio (Nu_{3r}/Nu_{1r}) lies in the range of 1.91 times to 3.42 times that of one side concave dimple roughened SAH.

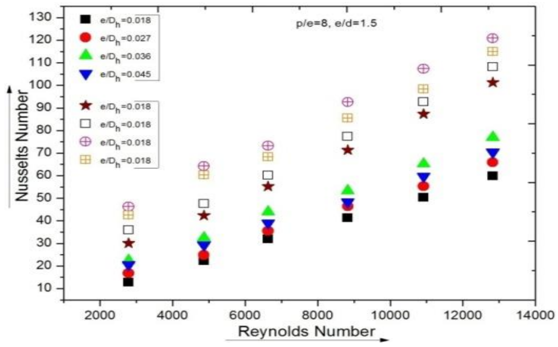

Figure 15. Variation in 'Nu' with 'Re' for different 'e/D_h' & for fixed 'p/e' = 8 & 'e/d'= 1.5

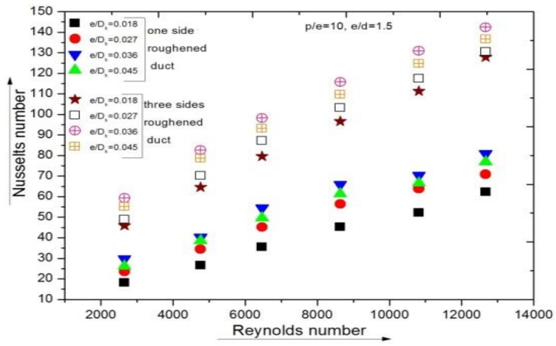

Figure 16. Variation in 'Nu' with 'Re' for different 'e/D_h' & for fixed 'p/e' = 10 & 'e/d'= 1.5

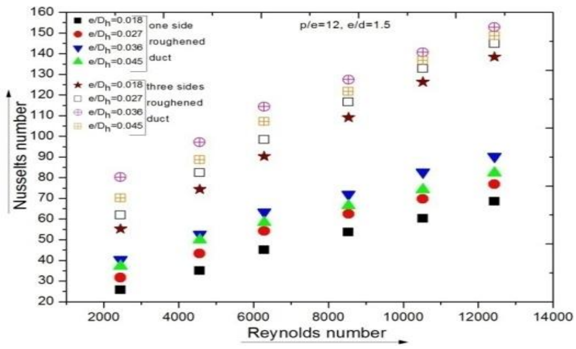

Figure 17. Variation in 'Nu' with 'Re' for different 'e/D_h' & for fixed 'p/e' = 12 & 'e/d'= 1.5

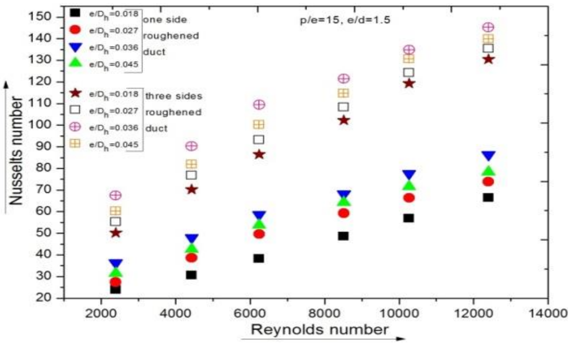

Figure 18. Variation in 'Nu' with 'Re' for different 'e/D_h' & for fixed 'p/e' = 15 & 'e/d'= 1.5

5.3. Effect of relative dimple depth ('e/d') on 'Nu'

Figs. 19 to 26 shows the augmentation in Nusselt number with increasing Re with respect to varying depth to diameter ratio at different sets of 'p/e' and 'e/D_h' values. Larger value of depth to diameter ratio (e/d>1.5) would not allow the flowing to escape quickly from the roughness element and reattach to the main primary flow. For e/d<1.5, air do not remain in contact with the roughness element for long enough time to achieve maximum possible heat transfer, thus velocities across dimples reduces, which may be insufficient to accelerate the flow through the dimple and hence the heat transfer may not increase significantly and also, due to insufficient space inside dimples, the obstruction to the flow may increase that could increase the friction factor across the ducts. Thus 'Nu' increases with an increase in depth to diameter ratio from 1 to 1.5 and attains maxima at e/d of 1.5 and thereafter it decreases with an increase in depth to diameter ratio.

The Nusselt number enhancement of the ducts roughened with concave dimple shape roughness element based on 'Nu' enhancement ratios (Nu_{3r}/Nu_{1r}) lies in the range of 3.09 times to 3.94 times that of the one side concave dimple roughened duct under similar operating conditions.

5.4. Effect of 'p/e' on friction factor

The variation in 'f' with 'Re' as a function of 'p/e' for fixed values of 'e/D_h' & 'e/d' is depicted in Figure 27-30 that clearly shows that 'f' decreases with increase in 'p/e' from 8.0 to 15.0 monotonously with increase in 'Re'.The maximum 'f' is observed at 'p/e' of 8.0 and its lowest value is observed at relative roughness pitch of 15.0 for both 1& 3-sides roughened ducts. The maximum enhancement in 'f' of three sides concave dimple roughened over those of one side roughened ones for varying ‘p/e’ was found to be as 1.62 to 2.79 times.

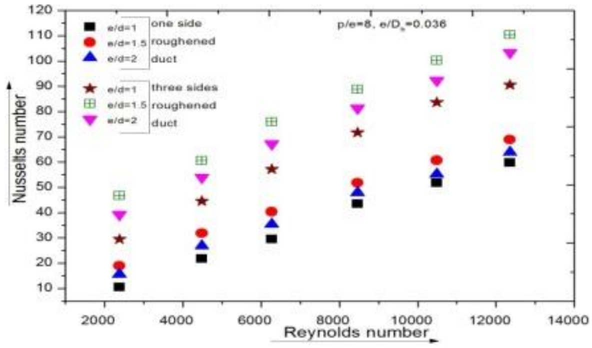

Figure 19. Variation in ‘Nu’ with ‘Re’ for different ‘e/d’ & for fixed ‘p/e’=8 & ‘e/D_h’= 0.036

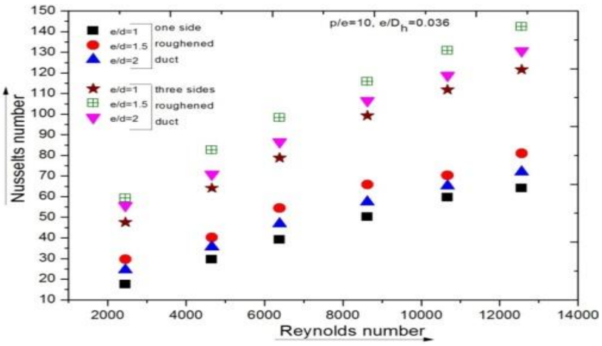

Figure 20. Variation in ‘Nu’ with ‘Re’ for different ‘e/d’ & for fixed ‘p/e’=10 & ‘e/D_h’ = 0.036

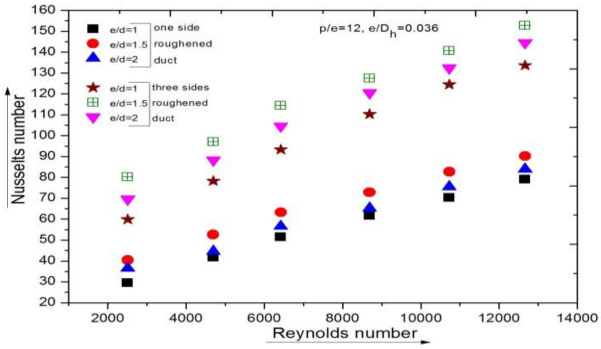

Figure 21. Variation in ‘Nu’ with ‘Re’ for different ‘e/d’ & for fixed ‘p/e’=12 & ‘e/D_h’=0.036

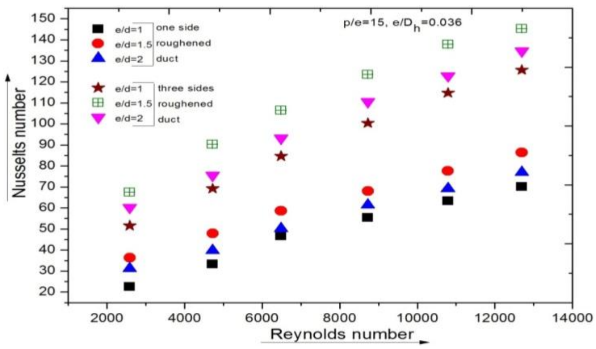

Figure 22. Variation in ‘Nu’ with ‘Re’ for different ‘e/d’ & for fixed ‘p/e’=15 & ‘e/D_h’=0.036

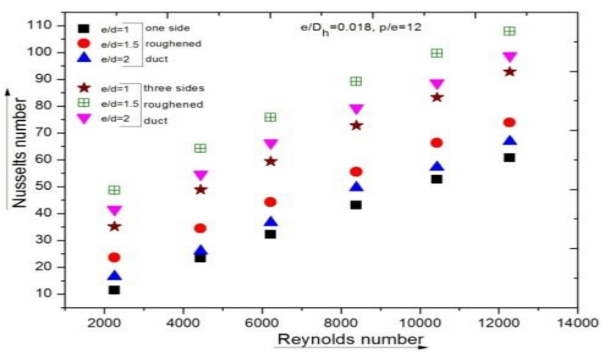

Figure 23. Variation in ‘Nu’ with ‘Re’ for different ‘e/d’ & for fixed ‘e/D_h’= 0.018 & ‘p/e’=12

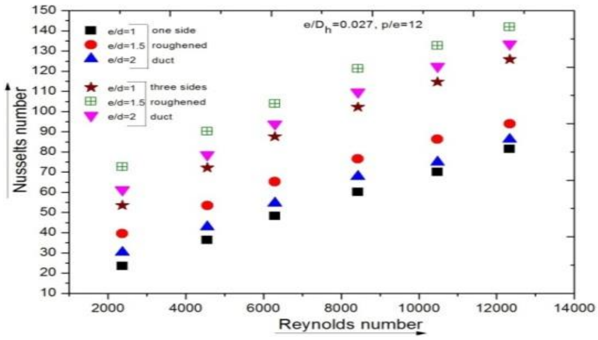

Figure 24. Variation in 'Nu' with 'Re' for different 'e/d' & for fixed 'e/D_h' =0.027 & 'p/e'=12

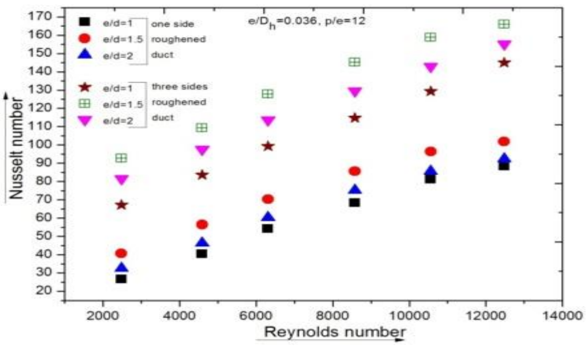

Figure 25. Variation in 'Nu' with 'Re' for different 'e/d' & for fixed 'e/D_h' =0.036 & 'p/e'=12

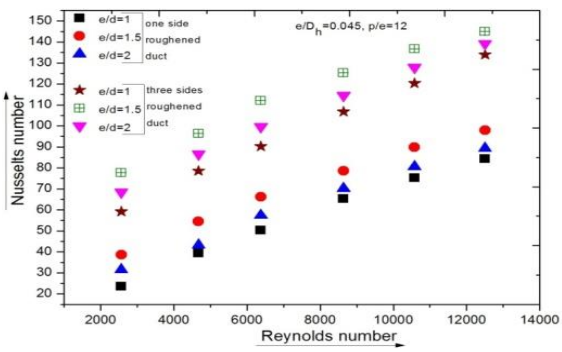

Figure 26. Variation in 'Nu' with 'Re' for different 'e/d' & for fixed 'e/D_h'=0.045 & 'p/e'=12

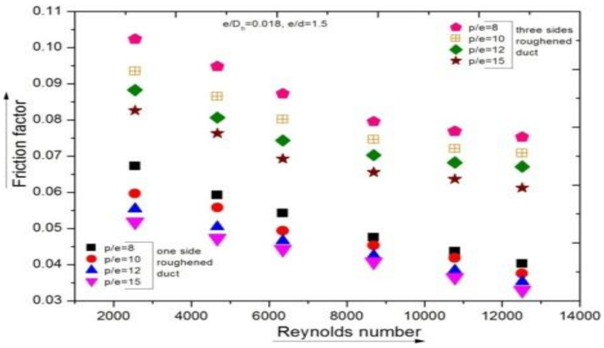

Figure 27. Variation in 'f' with Re for different 'p/e' & for fixed 'e/D$_h$' = 0.018 & 'e/d' = 1.5

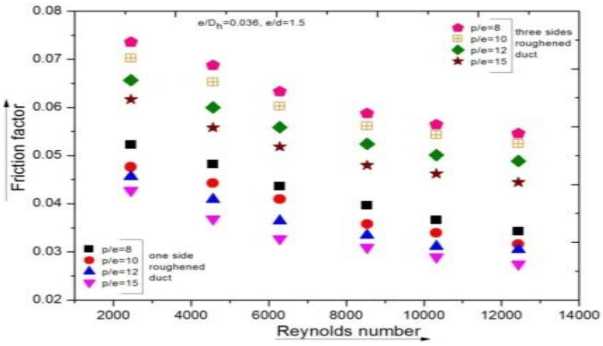

Figure 28. Variation in 'f' with Re for different 'p/e' & for fixed 'e/D$_h$' = 0.036 & 'e/d' = 1.5

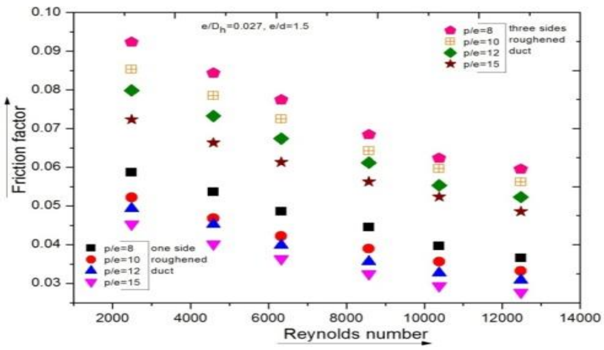

Figure 29. Variation in 'f' with Re for different 'p/e' & for fixed 'e/D$_h$' = 0.027 & 'e/d' = 1.5

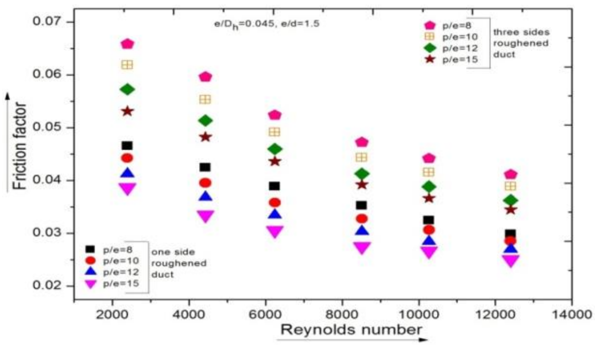

Figure 30. Variation in 'f' with Re for different 'p/e' & for fixed 'e/D_h' = 0.045 & 'e/d' = 1.5

5.5. Effect of 'e/D_h' on friction factor

The variation in 'f' with 'Re' for varying 'e/D_h' for fixed values of 'p/e' & 'e/d' is shown in Figure 31-34. Friction factor monotonously increases for both 1 & 3-sides roughened ducts with increase of 'e/D_h'. The increase in friction factor has occurred due to main flow impingement, formulation of vortex in the vicinity of dimples and also due to flow separation. Thus it may be concluded that the maximum & minimum value of 'f' in case of one & three sides concave dimple roughened ducts is observed for 'e/D_h' value of 0.045 & 0.018 respectively having 'p/e' 8 & relative dimple depth 1.5.

For 'e/D_h' 0.036-0.045, the augmentation in friction is very high; on the contrary 'Nu' decreases, causing unnecessary increase in pumping power as compared to heat transfer. The maximum enhancement in 'f' of three sides concave dimple roughened over those of one side roughened ones for varying 'p/e' was found to be as 1.52 to 2.34 times.

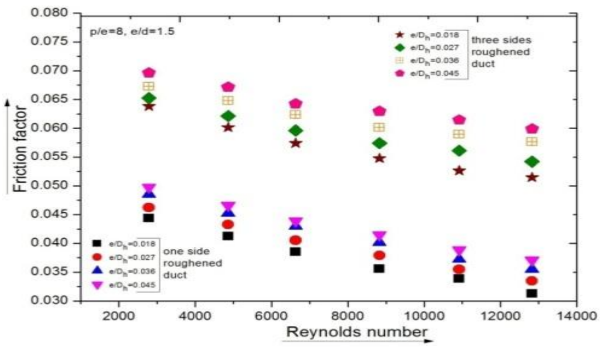

Figure 31. Variation in 'f' with 'Re' for different 'e/D_h' & for fixed 'p/e' = 8 & 'e/d' = 1.5

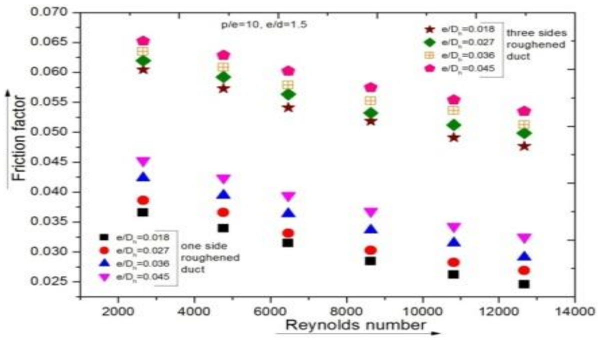

Figure 32. Variation in 'f' with 'Re' for different 'e/D_h' & for fixed 'p/e' = 10 & 'e/d' = 1.5

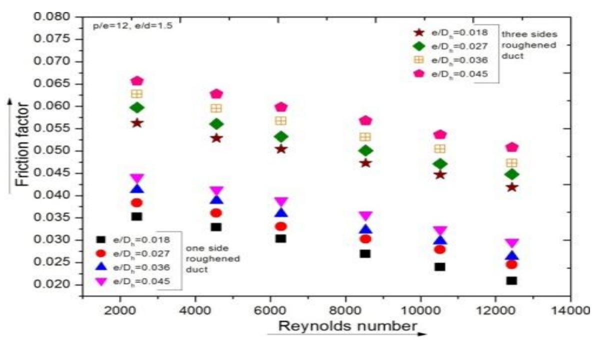

Figure 33. Variation in 'f' with 'Re' for different 'e/D_h' & for fixed 'p/e' = 12 & 'e/d' = 1.5

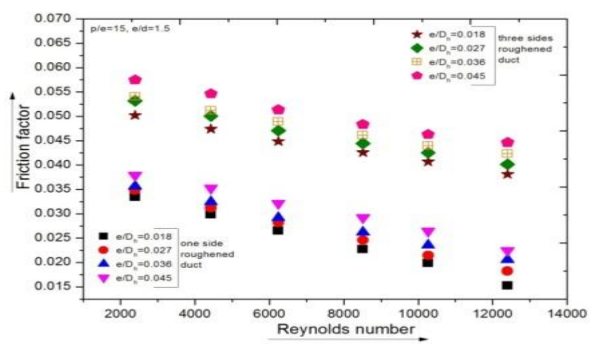

Figure 34. Variation in 'f' with 'Re' for different 'e/D_h' & for fixed 'p/e' = 15 & 'e/d' = 1.5

5.6. Effect of 'e/d' on friction factor

Figure 35 - 41 show the variation of 'f' with 'Re' for different values of depth to diameter ratio (e/d) at fixed values of 'p/e' or 'e/D_h'. The values of 'f' decreased with increase of depth to diameter ratio till 1.5 beyond which 'f' started increasing with increase in depth to diameter ratio. This may be due to the fact that at lower depth to diameter ratio (e/d < 1.5), all the dimples embossed upon the roughened surfaces take part in the flow and the pressure drop associated with the roughened ducts are assumed to be the cumulative effect of the entire dimples present on them. As the depth to diameter ratio is increased beyond this value (e/d > 1.5), some dimples may not participate in flow due to less vortices formation because of larger depth to diameter ratio. The minimum and maximum enhancement in 'f' of three sides concave dimple roughened over those of one side roughened ones for varying 'p/e' was found to be as 2.21 to 2.56 times.

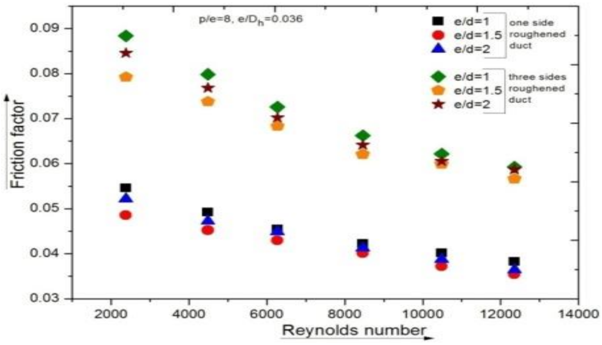

Figure 35. Variation in 'f' with 'Re' for different 'e/d' & for fixed 'p/e' =8 & 'e/D_h' = 0.036

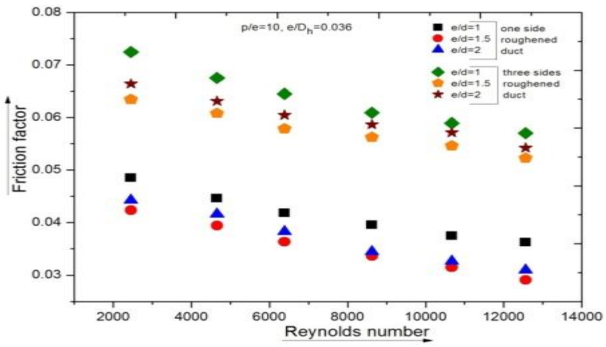

Figure 36. Variation in 'f' with 'Re' for different 'e/d' & for fixed 'p/e' =10 & 'e/D_h' = 0.036

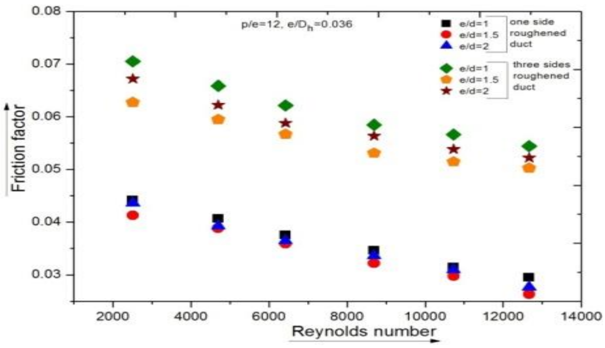

Figure 37. Variation in 'f' with 'Re' for different 'e/d' & for fixed 'p/e' =12 & 'e/D_h' = 0.036

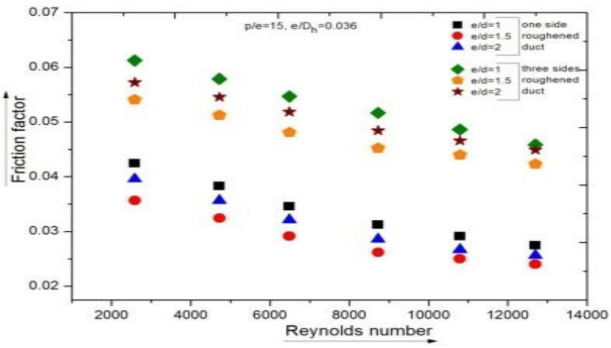

Figure 38. Variation in 'f' with 'Re' for different 'e/d' & for fixed 'p/e' =15 & 'e/D_h' = 0.036

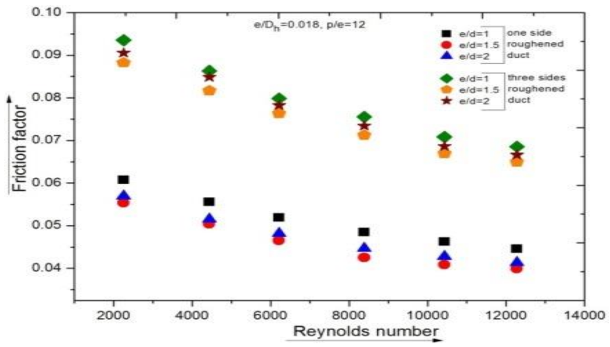

Figure 39. Variation in 'f' with 'Re' for different 'e/d' & for fixed 'e/D_h' = 0.018 & 'p/e' = 12

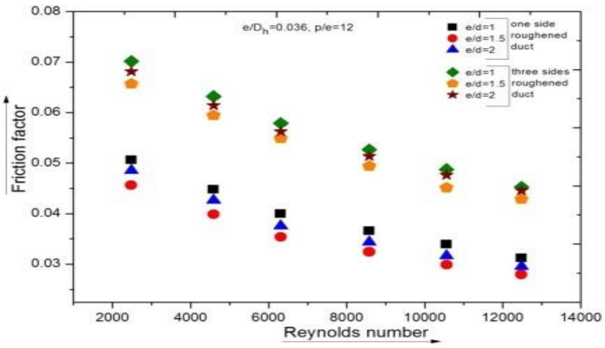

Figure 40. Variation in 'f' with 'Re' for different 'e/d' & for fixed 'e/D_h' = 0.036 & 'p/e' = 12

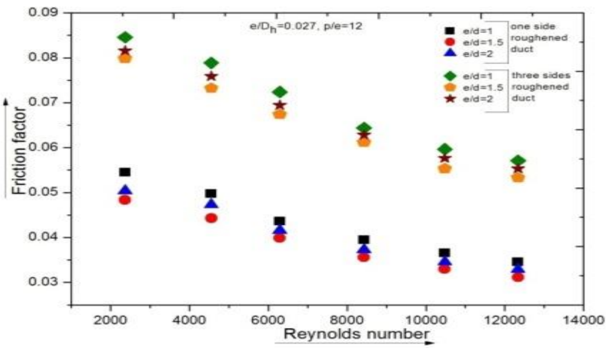

Figure 41. Variation in 'f' with 'Re' for different 'e/d' & for fixed 'e/D_h' = 0.027 & 'p/e' = 12

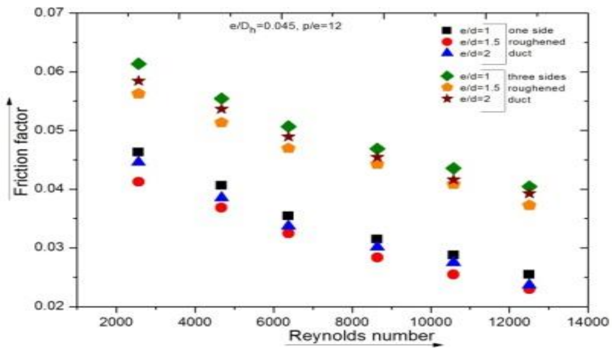

Figure 42. Variation in 'f' with 'Re' for different 'e/d' & for fixed 'e/D_h' = 0.45 & 'p/e' = 12

6. Conclusions

'Nu' & 'f' characteristics have been investigated of SAHs with roughened ducts by providing concave dimple shape geometry on one and three sides of the absorber plates. An exhaustive experimentation has been conducted to record experimental data for 'Nu' & 'f' characteristics in the range of system and operating parameters i.e. 'p/e', 'e/D_h', 'e/d' & 'Re'.

The effects produced by changing the roughness & operating parameters on 'Nu' & 'f' characteristics has been determined & a comparative study for performance of 3-sides & 1-side roughened SAHs with concave dimple roughness has been performed. The outcomes of the present investigations were conclusive & the same has been mentioned below:

(1) 'Nu' & 'f' varied as 'p/e', 'e/D_h' & 'e/d' were varied under the given operating range. In the entire range of 'Re' studied, 'Nu' increased as 'p/e' was increased from 8 to 12. On further increasing the value of 'p/e', 'Nu' started decreasing for both types of roughened ducts.

(2) A similar trend has been found in 'Nu' with the variation in 'e/D_h'. 'Nu' increased as the 'e/D_h' was increased from 0.018 to 0.036, beyond this, Nusselt number started decreasing with increase in e/D_h value for one and three sides roughened ducts.

(3) An increase in relative dimple depth, e/d resulted in an increase in Nusselt number from 1 to 1.5. Upon increasing e/d to 2, it was found 'Nu' value was less than so obtained at e/d value of 1.5 for both ducts.

(4) The maximum enhancement in 'Nu' for varying 'p/e', 'e/D_h' & 'e/d' was respectively found to be of the order of 2.6 to 3.55 times, 1.91 to 3.42 times and 3.09 to 3.94 times than one side concave dimple roughened duct for the parameters range investigated.

(5) Augmentation in Nusselt number is achieved along with friction factor rise across the roughened ducts. Friction has been found to decrease monotonously as the 'p/e' was increased from 8 to 12 for both the roughened ducts.

(6) With the variation of 'e/D_h' from 0.018 to 0.045, the values of 'f' increased monotonously with variation in flow and other roughness parameters for one as well as three sides roughened ducts.

(7) As 'e/d' was varied from 1 to 2, the values of friction factor decreased as the e/d values were varied from 1 to 1.5 and then the values of friction factor increased as the e/d values were further increased from 1.5 to 2 for 1 as well as 3-sides concave dimple roughened SAH.

(8) Minimum and maximum enhancement in the values of 'f' of 3-sides concave dimple over those of 1-side roughened ones for varying 'p/e', 'e/D_h' & 'e/d' was respectively found to be as 1.62 to 2.79 times, 1.52 to 2.34 times and 2.21 to 2.56 times.

References

Ahn S. W. (2001). The effect of roughness types on friction factor and heat rectangular duct. *Int Commun Heat Mass Transf.*, Vol. 28, pp. 933-942. http://dx.doi.org/10.1016/s0735-1933(01)00297-4

Akhtar N., Mullick S.C. (2012). Effect of absorption of solar radiation in glass-cover(s) on heat transfer coefficients in upward heat flow in single and double glazed flat-plate collectors. *International Journal of Heat and Mass Transfer*, Vol. 55, No. 1-3, pp. 125-132. http://dx.doi.org/10.1016/j.ijheatmasstransfer.2011.08.048

Armaroli N., Balzani V. (2016). Solar Electricity and Solar Fuels: Status and Perspectives in the Context of the Energy Transition. *Chemistry-A European Journal*, Vol. 22, pp. 32-57. http://dx.doi.org/10.1002/chin.201611269

ASHRAE Standard 93-97 (1977). Methods of testing to determine the thermal performance of solar collectors. American Society of Heating, Refrigerating and Air-conditioning Engineers Inc., Atlanta Ga.

Bhagoria J. S., Saini J. S., Solanki S. C. (2002). Heat transfer co-efficient and friction factor correlation for rectangular solar air heater duct having transverse wedge shaped rib roughness on the absorber plate. *Renewable Energy*, Vol. 25, pp. 341-369. http://dx.doi.org/10.1016/s0960-1481(01)00057-x

Chang S. W., Liou T. M., Chiang K. F., Hong G. F. (2008). Heat transfer and pressure drop in rectangular channel with compound roughness of V-shaped ribs and deepened scales. *International Journal of Heat Mass Transfer*, Vol. 51, pp. 457-468. http://dx.doi.org/10.1016/j.ijheatmasstransfer.2007.05.010

Dippreyy D. F., Sabersky R. H. (1963). Heat and momentum transfer in smooth and rough tubes at various Prandtl numbers. *Int J Heat Mass Transf.*, Vol. 6, pp. 329-53. http://dx.doi.org/10.1016/0017-9310(63)90097-8

Duffie J. A., Beckman W. A. (1991). *Solar Engineering Thermal Processes*, John Wiley, New York.

Edwards F. J., Sheriff N. (1961). The heat transfer and friction characteristics for forced convection air flow over a particular type of rough surface. *Int Dev Heat Transf. ASM*E, pp. 415-425.

Firth R. J., Meyer L. (1983). A comparison of the heat transfer and friction factor performance of four different types of artificially roughened surface. *Int J Heat Mass Transf.*, Vol. 26, No. 2, pp. 175-83. http://dx.doi.org/10.1016/s0017-9310(83)80024-6

Gupta D., Solanki S. C., Saini J. S. (1997). Thermohydraulic performance of solar air heaters with roughened absorber plates. *Solar Energy*, Vol. 61, pp. 33-42. http://dx.doi.org/10.1016/s0038-092x(97)00005-4

Han J. C., Park J. S., Lei C. K. (1985). Heat transfer enhancement in channel with turbulence promoters. *ASME Journal Engineering for Gas Turbine and Power*, Vol. 107, pp. 628-635. http://dx.doi.org/10.1115/1.3239782

Han J. C., Zhang Y. M., Lee C. P. (1991). Augmented heat transfer in square channels with parallel, crossed, and V shaped angled ribs. ASME Journal of Heat Transfer, Vol. 113, pp. 590-596. http://dx.doi.org/10.1115/1.2910606

Karwa R., Solanki S., Saini J. (2001). Thermo-hydraulic performance of solar air heaters having integral chamfered rib roughness on absorber plates. *Energy*, Vol. 26, No. 2, pp. 161-176. http://dx.doi.org/10.1016/S0360-5442(00)00062-1

Kline S. J., Mcclintock F. A. (1953). Describing uncertainties in single sample experiments. *Mech Eng.*, Vol. 75, pp. 3-8.

Naphon P. (2008). Effect of corrugated plates in an in-phase arrangement on the heat transfer and flow developments. *International Journal of Heat Mass Transfer*, Vol. 51, pp. 3963-3971. http://dx.doi.org/10.1016/j.ijheatmasstransfer.2007.11.050

Nguyen T. M., Khodadadi J. M., Vlachos N. S. (1989). Laminar flow and conjugate heat transfer in rib roughened tubes. *Numerical Heat Transfer Applications*, Vol. 15, pp. 165-79. http://dx.doi.org/10.1080/10407788908944683

Patil A. K., Saini J. S., Kumar K. (2012). Heat transfer and friction characteristics of solar air heater duct roughened by discrete V-shape ribs combined with staggered rib piece. *J Renew Sustain Energy*, Vol. 4, pp. 13115. http://dx.doi.org/10.1063/1.3682072

Pillar P. K., Agarwal R. C. (1981). Factors influencing solar energy collector efficiency. *Applied Energy*, Vol. 8, pp. 205-213. http://dx.doi.org/10.1016/0306-2619(81)90018-0

Prasad B. N., Saini J. S. (1988). Effect of artificial roughness on heat transfer and friction factor in a solar air heater. *Solar Energy*, Vol. 41, No. 6, pp. 555-560. http://dx.doi.org/10.1016/0038-092X(88)90058-8

Prasad K., Mullick S. C. (1985). Heat transfer characteristics of a solar air heater used for drying purposes. *Applied Energy*, Vol. 13, pp. 83-93. http://dx.doi.org/10.1016/0306-2619(83)90001-6

Saini R. P., Verma J. (2008). Heat transfer and friction correlations for a duct having dimple shape artificial roughness for solar air heater. *Energy*, Vol. 33, pp. 1277-1287. http://dx.doi.org/10.1016/j.energy.2008.02.017

Singh S., Chander S., Saini J. S. (2012). Investigations on thermo-hydraulic performance due to flow-attack-angle in V-down rib with gap in a rectangular duct of solar air heater. *Appl Energy*, Vol. 97, pp. 907-912. http://dx.doi.org/10.1016/j.apenergy.2011.11.090

Singh S., Chander S., Saini J. S. (2015). Thermo-hydraulic performance due to relative roughness pitch in V-down rib with gap in solar air heater duct-Comparison with similar rib roughness geometries. *Renewable and Sustainable Energy Reviews*, Vol. 43, pp. 1159-1166. http://dx.doi.org/10.1016/j.rser.2014.11.087

Skullong S., Promvonge P. (2014). Experimental Investigation on Turbulent Convection in Solar Air Heater Channel Fitted with Delta Winglet Vortex Generator. *Chinese Journal of Chemical Engineering*, Vol. 22, No. 1, pp. 1-10. http://dx.doi.org/10.1016/S1004-9541(14)60030-6

Sukhatme S. P. (1986). *Solar Energy Engineering*, Prentice Hall Inc., New Jersey.

Varun Saini, R. P. Singal S. K. (2007). A review of roughness geometry used in solar air heaters. *Sol Energy*, Vol. 81, pp. 1340-50. http://dx.doi.org/10.1016/j.solener.2007.01.017

Yadav A. S., Bhagoria J. L. (2014). A CFD based thermo-hydraulic performance analysis of an artificially roughened solar air heater having equilateral triangular sectioned rib roughness on the absorber plate. *International Journal of Heat and Mass Transfer*, Vol. 70, pp. 1016-1039. http://dx.doi.org/10.1016/j.ijheatmasstransfer.2013.11.074

Nomenclatures

Parameters	Symbol	Unit
Area of orifice of orifice plate	A_o	m^2
Area of absorber plate	A_p	m^2
Specific heat capacity of air	C_p	J/kgK
Length of SAH duct	L	m
Width of SAH duct	W	m
Height of SAH duct	H	m
Mass flow rate of air	$\dot{m}$	Kg/s
Thermal conductivity of air	k	W/mk
Test section pressure drop	Δp_d	N/m^2
Orifice meter pressure drop	Δp_o	N/m^2
Useful heat gain	Q_u	W
Mean absorber plate temperature	T_{pm}	˚C
Mean air temperature in the duct	T_{fm}	˚C
Average velocity of air through the duct	v_d	m/s
Coefficient of discharge	C_d	-
Hydraulic diameter of duct	D_h	mm
Dimple pitch	p	mm
Dimple depth/height	e	mm
Dimple diameter	d	mm
Solar air heater	SAH	-
Cross-section	c/s	-
versus	v/s	-
Dynamic viscosity of air	μ	N s/m^2
Kinematic viscosity of air	ν	m^2/s

Dimensionless parameters

Name of parameter	Symbol
Relative dimple pitch	p/e
Relative dimple height	e/D_h
Relative dimple depth	e/d
Friction factor	f
Friction factor for smooth surface	f_s
Friction factor for one side roughened duct	f_{1r}
Friction factor for three sides roughened duct	f_{3r}
Nusselt number	Nu
Nusselt number for one side roughened duct	Nu_{1r}
Nusselt number for three sides roughened duct	Nu_{3r}
Reynolds number	Re
Aspect ratio of collector duct	W/H

APPENDIX-A

Uncertainty Analysis

The experimental data recorded during investigation often differ from the actual data due to a lot of unaccountable factors while performing experiments. This deviation of the recorded data from actual data is called as uncertainty. The uncertainty is determined using method suggested by Klein and McClintock. The procedure for the evaluation of uncertainty has been discussed below:

Let a parameter be calculated using certain measured quantities as,

$y = y(x_1, x_2, x_3, \ldots\ldots, x_n)$

Then uncertainty in measurement of y is given as follows:

$$\delta_y = \left[\left(\frac{\delta_y}{\delta_{x_1}} \delta_{x_1} \right)^2 + \left(\frac{\delta_y}{\delta_{x_2}} \delta_{x_2} \right)^2 + \left(\frac{\delta_y}{\delta_{x_3}} \delta_{x_3} \right)^2 + \ldots\ldots\ldots + \left(\frac{\delta_y}{\delta_{x_n}} \delta_{x_n} \right)^2 \right]^{0.5} \quad (1)$$

Where δ_{x1}, δ_{x2}, δ_{x3}, …, δ_{xn} are the possible errors in measurements of x_1, x_2, x_3 …x_n.

δ_y is absolute uncertainty and δ_y/y is relative uncertainty.

Uncertainty in the measurement of various parameters:

1. Area of flow, plate and orifice meter

$$\frac{\delta A_p}{A_p} = \left[\left(\frac{\delta L}{L} \right)^2 + \left(\frac{\delta W}{W} \right)^2 \right]^{0.5} \quad (2)$$

Area of absorber plate (A_p):

$$A = W \times L$$

$$\frac{\delta A_p}{A_p} = \left[\left(\frac{1.1}{1500} \right)^2 + \left(\frac{0.06}{250} \right)^2 \right]^{0.5}$$

$$= 7.71 \text{ x } 10^{-4}$$

$$= 0.0007716$$

Area of flow (A_{flow}):

$$\frac{\delta A_{flow}}{A_{flow}} = \left[\left(\frac{\delta H}{H} \right)^2 + \left(\frac{\delta W}{W} \right)^2 \right]^{0.5} \quad (3)$$

Cross sectional area of air flow duct (A):

$$\frac{\delta A}{A} = \left[\left(\frac{\delta H}{H}\right)^2 + \left(\frac{\delta W}{W}\right)^2\right]^{0.5}$$

$$\frac{\delta A}{A} = \left[\left(\frac{0.04}{25}\right)^2 + \left(\frac{0.06}{250}\right)^2\right]^{0.5}$$

$$= 1.617 \text{ x } 10^{-3}$$

$$= 0.001617$$

Area of orifice meter (A_o):

$$\frac{\delta A_o}{A_o} = \left[\frac{\left(\frac{\pi D_o \times \delta D_o}{2}\right)}{\frac{\pi D_o{}^2}{4}}\right]^{0.5} \tag{4}$$

$$\frac{\delta A_o}{A_o} = \left[\frac{2\delta D_o}{D_o}\right]$$

$$\frac{\delta A_o}{A_o} = \left[\frac{2 \times 0.04}{38}\right]$$

$$= 2.10 \text{ x } 10^{-3}$$

$$= 0.002105$$

2. Hydraulic diameter

$$\frac{\delta D_h}{D_h} = \frac{\left[\left(\frac{\delta D_h \delta W}{W}\right)^2 + \left(\frac{\delta D_h \delta H}{H}\right)^2\right]^{0.5}}{\left[2\left(W \times H\right)\left(W + H\right)\right]^{-1}} \tag{5}$$

$$\frac{\delta D_h}{D_h} = \frac{\left[\left(\frac{0.04 \times 0.06}{250}\right)^2 + \left(\frac{0.04 \times 0.04}{25}\right)^2\right]^{0.5}}{\left[2\left(250 \times 25\right)\left(250 + 25\right)\right]^{-1}}$$

$$= 2.231 \text{ x } 10^{-3}$$

$$= 0.002321$$

3. Density

$$\frac{\delta \rho_a}{\rho_a} = \left[\left(\frac{\delta P_a}{P_a} \right)^2 + \left(\frac{\delta T_o}{T_o} \right)^2 \right]^{0.5} \tag{6}$$

$$\frac{\delta \rho_a}{\rho_a} = \left[\left(\frac{0.2}{101} \right)^2 + \left(\frac{0.41}{39} \right)^2 \right]^{0.5}$$

= 0.00106

4. Mass flow rate

$$\frac{\delta \dot{m}}{\dot{m}} = \left[\left(\frac{\delta C_d}{C_d} \right)^2 + \left(\frac{\delta A_o}{A_o} \right)^2 + \left(\frac{\delta \rho_a}{\rho_a} \right)^2 + \left(\frac{\delta \Delta P_o}{P_o} \right)^2 \right]^{0.5} \tag{7}$$

$$\frac{\delta \dot{m}}{\dot{m}} = \left[\left(\frac{0.005}{0.62} \right)^2 + \left(0.002105 \right)^2 + \left(0.00106 \right)^2 + \left(\frac{0.14}{354} \right)^2 \right]^{0.5}$$

= 8.411 x 10^{-3}

= 0.008411

5. Velocity of air through test section

$$V = \frac{\dot{m}}{\rho (WH)} \tag{8}$$

$$\frac{\delta V}{V} = \left[\left(\frac{\delta \dot{m}}{\dot{m}} \right)^2 + \left(\frac{\delta \rho}{\rho} \right)^2 + \left(\frac{\delta W}{W} \right)^2 + \left(\frac{\delta H}{H} \right)^2 \right]^{0.5}$$

$$\frac{\delta V}{V} = \left[\left(0.008411 \right)^2 + \left(0.00106 \right)^2 + \left(\frac{0.06}{250} \right)^2 + \left(\frac{0.04}{25} \right)^2 \right]^{0.5}$$

= 8.63 x 10^{-3}

= 0.00863

6. Reynolds Number (Re)

$$\mathrm{Re} = \frac{\rho V D_h}{\mu} \tag{9}$$

$$\frac{\delta \mathrm{Re}}{\mathrm{Re}} = \left[\left(\frac{\delta V}{V} \right)^2 + \left(\frac{\delta \rho}{\rho} \right)^2 + \left(\frac{\delta D_h}{D_h} \right)^2 + \left(\frac{\delta \mu}{\mu} \right)^2 \right]^{0.5}$$

$$\frac{\delta \mathrm{Re}}{\mathrm{Re}} = \left[(0.00863)^2 + (0.00106)^2 + (0.002321)^2 + \left(\frac{0.002}{1.89} \right)^2 \right]^{0.5}$$

$$= 9.061 \text{ x } 10^{-3}$$

$$= 0.009061$$

7. Useful heat gain

$$\frac{\delta Q_u}{Q_u} = \left[\left(\frac{\delta \dot{m}}{\dot{m}} \right)^2 + \left(\frac{\delta C_p}{C_p} \right)^2 + \left(\frac{\delta \Delta T}{\Delta T} \right)^2 \right]^{0.5} \tag{10}$$

$$\frac{\delta Q_u}{Q_u} = \left[(0.008411)^2 + \left(\frac{1.4}{1005} \right)^2 + \left(\frac{0.68}{22.48} \right)^2 \right]^{0.5}$$

$$= 0.03142$$

8. Thermal Efficiency

$$\frac{\delta \eta_{th}}{\eta_{th}} = \left[\left(\frac{\delta Q_u}{Q_u} \right)^2 + \left(\frac{\delta I}{I} \right)^2 + \left(\frac{\delta A_p}{A_p} \right)^2 \right]^{0.5} \tag{11}$$

$$\frac{\delta \eta_{th}}{\eta_{th}} = \left[(0.03142)^2 + \left(\frac{0.94}{972} \right)^2 + (0.0007716)^2 \right]^{0.5}$$

$$= 0.03144$$

9. Heat transfer co-efficient (h)

$$\frac{\delta h}{h} = \left[\left\{ \frac{\delta Q}{Q} \right\}^2 + \left\{ \frac{\delta A_p}{A_p} \right\}^2 + \left\{ \frac{\delta \left(T_{pm} \right)}{\left(T_{pm} \right)} \right\}^2 \right]^{0.5} \quad (12)$$

$$\frac{\delta h}{h} = \left[\left\{ 0.03144 \right\}^2 + \left\{ 0.0007716 \right\}^2 + \left\{ \frac{0.19}{\left(28.13 \right)} \right\}^2 \right]^{0.5}$$

$$= 0.03724$$

10. Nusselt number (Nu)

$$\frac{\delta Nu}{Nu} = \left[\left\{ \frac{\delta h}{h} \right\}^2 + \left\{ \frac{\delta D_h}{D_h} \right\}^2 + \left\{ \frac{\delta \left(k \right)}{\left(k \right)} \right\}^2 \right]^{0.5} \quad (13)$$

$$\frac{\delta Nu}{Nu} = \left[\left\{ 0.03724 \right\}^2 + \left\{ 0.002321 \right\}^2 + \left\{ \frac{\delta \left(0.00001 \right)}{\left(0.02652 \right)} \right\}^2 \right]^{0.5}$$

$$= 0.04167$$

11. Friction factor (f)

$$\frac{\delta f}{f} = \left[\left\{ \frac{\delta \left(\Delta p_d \right)}{\left(\Delta p_d \right)} \right\}^2 + \left\{ \frac{\delta D_h}{D_h} \right\}^2 + \left\{ \frac{\delta \left(L \right)}{L} \right\}^2 + \left\{ \frac{\delta \left(V \right)}{V} \right\}^2 + \left\{ \frac{\delta \left(\rho \right)}{\rho} \right\}^2 \right]^{0.5} \quad (14)$$

$$\frac{\delta f}{f} = \left[\left\{ \frac{\left(0.01 \right)}{\left(10 \right)} \right\}^2 + \left\{ 0.002321 \right\}^2 + \left\{ \frac{\left(0.87 \right)}{1500} \right\}^2 + \left\{ 0.00863 \right\}^2 + \left\{ 0.00106 \right\}^2 \right]^{0.5}$$

$$= 0.\ 04389$$

The uncertainty analysis has been carried out for the entire set of parameter investigated within the operating range and the uncertainty variation of various parameters obtained is presented in Table 2.